PHYSICAL REVIEW D VOLUME 36, NUMBER 3 1 AUGUST 1987

Measurement of the ratio of Σ^0 to Λ^0 inclusive production from 28.5-GeV/c protons on beryllium

Marilyn W. Sullivan,* Douglas A. Jensen, Michael N. Kreisler,
Martin Marcin,† and Kamal K. Raychaudhuri*
Department of Physics and Astronomy, University of Massachusetts, Amherst, Massachusetts 01003

Gerry M. Bunce, Yousef Makdisi, and Peter Yamin
Accelerator Department, Brookhaven National Laboratory, Associated Universities, Inc., Upton, New York 11973

Edmond C. Dukes and Oliver E. Overseth
Department of Physics, University of Michigan, Ann Arbor, Michigan 48109

Kenneth Heller
School of Physics and Astronomy, University of Minnesota, Minneapolis, Minnesota 55455
(Received 12 February 1987)

The ratio of the cross section for Σ^0 inclusive production to the cross section for Λ^0 inclusive production has been measured with 28.5-GeV/c protons incident on a beryllium target at an average laboratory production angle of 4°. This ratio was measured to be $0.278\pm0.011\pm0.05$, where the uncertainties are statistical and systematic in that order. The ratio does not depend strongly on the momentum of the produced particle between 10 and 24 GeV/c. The effect of Σ^0 contamination on previous determinations of the polarization of inclusively produced Λ^0's is discussed.

I. INTRODUCTION

An interesting question in the study of the hadronic production of hyperons is whether such processes depend on spin. One might naively expect that particles produced in a high-energy collision would lose all memory of the initial state. However, studies of the inclusive production of hyperons disagree with that expectation. Specifically, significant polarization of hyperons in the final state has been observed.[1–10] Such polarizations indicate that spin must play an essential role in hyperon production. But, despite a great deal of both experimental and theoretical[11–14] effort, there is no satisfactory explanation for this behavior and further experimental input is required.

To that end, we conducted an experimental study of the inclusive production of both Σ^0 and Λ^0 hyperons. Since both hyperons have the same quark constituents, albeit with different internal spin structure, a comparison of the two production processes could yield clues to the specific nature of the spin-dependent mechanisms. In addition to the direct comparison, a measurement of Σ^0 and Λ^0 production would unravel another aspect of this area of investigation. In previous measurements of Λ^0 production and polarization, no distinction was made between Λ^0's produced directly and Λ^0's resulting from the decay of other particles (such as the Σ^0) or resonances. No picture of Λ^0 polarization could be complete without an examination of such "dilution" factors.

In this paper, we present the details of that experimental program which yielded the first measurement of the ratio of the inclusive production of Σ^0 hyperons to the inclusive production of Λ^0 hyperons using 28.5-GeV/c protons. These results have been reported earlier in a shorter form.[15]

As indicated above, this experimental program was motivated in large measure by the surprising observation that Λ^0's have significant polarization when produced in high-energy interactions. That polarization increases with the transverse momentum of the Λ^0 relative to the incident-beam direction. Thus, the phenomenon may be probing some fundamental characteristic of the production process. For that reason, experiments have been performed on other hyperons.[16–18] Although these studies have shown that the polarization phenomenon is not limited to the Λ^0 and although the polarized hyperons have been useful in several ingenious experiments,[19] extremely little is known about the mechanism causing the polarization.

In addition, the polarization measurements on Λ^0's have been performed on inclusively produced hyperons where no distinction was made between Λ^0's produced directly in the strong-interaction process, Λ^0's which are the daughters of strong resonances such as the $\Sigma(1385)$, and Λ^0's which are the decay produces of other weakly decaying particles such as the Σ^0, Ξ^0, or Ξ^-. Such lack of information greatly complicates the task of understanding or modeling the phenomenon—if it does not render such a task impossible. The experiment described here was performed to resolve a portion of that confusion.

Although this experiment was the first to compare Σ^0 and Λ^0 inclusive production by protons in this energy range, there have been other experiments which have dealt with closely related issues. In a measurement of low-energy exclusive processes,[20] the reactions $p+p\rightarrow\Lambda^0K^+p$ and $p+p\rightarrow\Sigma^0K^+p$ were compared using protons at 6 GeV/c. The cross section for the Σ^0 production reaction was found to be approximately $\frac{1}{3}$ of the cross section for the Λ^0 production reaction. Obviously the extrapolation

 ©1987 The American Physical Society

of this ratio of low-energy exclusive cross sections to higher-energy inclusive studies is difficult but the size of the Σ^0 production cross section reinforces the need for measurements at higher energies. In $K^- p$ interactions at 8.25 GeV/c (Ref. 6), Σ^0 production was found to be almost 30% of Λ^0 production. We note the interesting agreement with the lower-energy exclusive measurement in pp interactions. Finally, several studies of baryon resonance production at different energies[6,21] indicate that a reasonably large fraction of Λ^0's are the decay products of such resonances, e.g., the $\Sigma(1385)$.

Such experimental hints have not slowed attempts to calculate the Σ^0/Λ^0 production ratios—even though the production process may in fact be extremely complex. For example, using a model in which quark recombination occurs according to the coefficients of hadronic SU(6) wave functions, DeGrand and Miettinen[14] have calculated the Σ^0 to directly produced Λ^0 ratio to be 0.11. In the model, both Σ^0 and Λ^0 production involve fragments of the proton projectile combining with a strange quark from the quark sea. A value for the Σ^0-to-Λ^0 production ratio closer to unity is predicted from the naive observation that inclusive production cross sections for processes with the same quark content in projectile and product are the same—*ignoring* spin-dependent mechanisms.

In the following we present the details of the experiment, the analysis procedure, the results, a comparison with various theoretical models, and a discussion of the effect of this measurement on previous studies of Λ^0 polarization.

II. THE EXPERIMENT

This measurement was performed at the Brookhaven National Laboratory Alternating Gradient Synchrotron (AGS). The beam line and much of the apparatus have been used for studies of both rare Λ^0 decays[22] and Λ^0 and $\overline{\Lambda}^0$ polarization.[2,16] Since they have been described in detail in those papers and elsewhere,[23,24] the discussion here will be somewhat abbreviated.

A beam of 28.5-GeV/c protons extracted from the AGS ring was focused on the $B5$ target, a piece of beryllium 15 cm long with a 2.5-mm-square cross section. The location and intensity of the proton beam were monitored by an ion chamber and segmented-wire ion chambers. The proton beam was delivered in spills of 1.2-sec duration every 2.5 sec with a typical intensity of 6×10^8 protons/spill.

A neutral beam was defined at an angle of 4° horizontally from the proton beam axis by a brass collimator embedded in the gap of a 1.83-m-long magnet ($B5D5$). See Fig. 1. The cross section of the collimator was tapered, 3.8×5.1 cm^2 at the entrance expanding to 12.7×13.2 cm^2 at the exit. The design of the collimator was chosen to maximize the acceptance for the photons from Σ^0 decay. The field integral in $B5D5$ was 3.71 T m, sufficient to sweep charged particles from the beam. This magnetic field also played a crucial role in reducing systematic biases. The magnetic field, oriented in a horizontal direction, precessed the Λ^0 spin. The polarity of the magnetic field was reversed periodically to maintain an equal number of events in each setting of the field.

The neutral beam then entered a decay region, a trapezoidal wooden box encased in concrete and steel and lined with an 0.76-mm-thick Mylar bag. The region was filled with helium at atmospheric pressure to minimize interactions. A scintillator veto counter at the upstream end of the decay region (the veto counter V) was used to eliminate triggers in which charged particles entered the region. Charged particles resulting from decays occurring in the decay region were detected and momentum analyzed in the spectrometer located just downstream of the decay region. Λ^0 hyperons were identified via the decay $\Lambda^0\to p+\pi^-$ while Σ^0 hyperons were identified via the decay $\Sigma^0\to\Lambda^0+\gamma$. The spectrometer, which will be described below, was designed to enhance the acceptance for the $\Lambda^0\to p+\pi^-$ decay mode over other decays and over the decays of other weakly decaying particles (such as K^0's). The photon from the Σ^0 decay was detected and measured in an array of lead-glass blocks.

Plan and elevation views of the spectrometer appear in Figs. 1 and 2. The coordinate system for the spectrome-

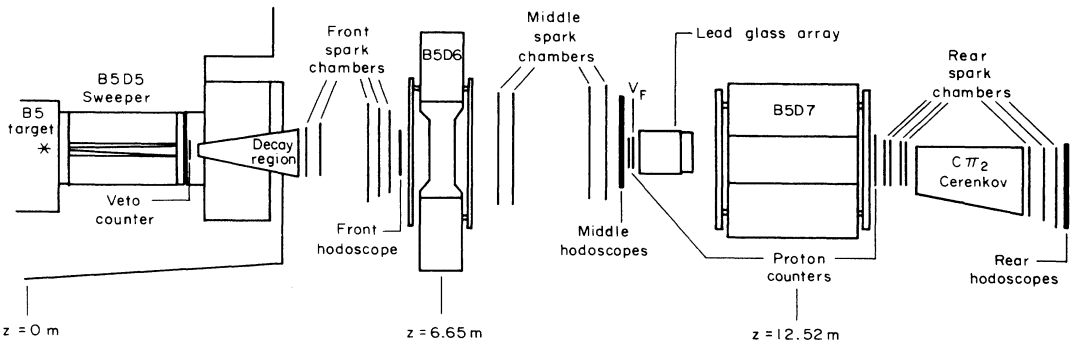

FIG. 1. Plan view of the spectrometer. The 28.5-GeV/c proton beam was transported to and focused upon the $B5$ target by an array of dipoles and quadrupole magnets. A collimator in the gap of the sweeping magnet $B5D5$ removed charged particles from the neutral beam and determined the aperture of the beam. Particles were then detected and measured in a spectrometer with 28 planes of spark chambers, several scintillation-counter hodoscopes, a lead-glass array for photon detection, and two analyzing magnets—$B5D6$ and $B5D7$.

TABLE I. Apertures, positions, and thickness of detector elements. Thicknesses are given in fractions of a radiation length including the appropriate lengths of air.

Name and description	Apertures x (cm)	Apertures y (cm)	z (m)	L/L_{rad}
Target			0.000	
Collimator entrance	±1.91	±2.54	0.508	
Collimator exit	±12.70	−10.67,2.54	2.337	
V veto counter	±15.24	−15.24,5.08	2.413	0.0163
Decay-region entrance	±15.24	−12.70,5.08	2.616	0.0004
Decay-region exit	±40.64	±20.32	4.267	0.0004
SFXY1 spark chamber	±48.26	±22.86	4.521	0.0019
SFXY2 spark chamber	±48.26	±22.86	4.696	0.0027
SFUV3 spark chamber	±71.12(u)	±48.26(v)	5.405	0.0027
SFXY4 spark chamber	±76.20	±25.40	5.565	0.0018
SFXY5 spark chamber	±76.20	±25.40	5.738	0.0018
HFX counter hodoscope	−41.68,40.51	±22.86	5.932	0.0079
$B5D6$ $72D18$ entrance	±91.44	−31.12,29.85	6.425	
$B5D6$-$72D18$ exit	±91.44	−31.12,29.85	6.882	
SMXY1 spark chamber	±76.20	±38.10	7.583	0.0041
SMXY2 spark chamber	±76.20	±38.10	7.825	0.0034
SMXY3 spark chamber	−58.42,93.98	±38.10	9.060	0.0034
SMXY4 spark chamber	−58.42,93.98	±38.10	9.327	0.0017
HMX counter hodoscope	−62.23,90.17	±40.64	9.444	0.0163
HMB counter hodoscope	−62.23,90.17	±40.64	9.552	0.0307
P counter	−28.58,17.15	−16.51,12.70	9.660	0.0206
HMS counter hodoscope	−25.78,19.94	±11.43	9.670	0.0048
V_F lead-glass veto counter	−36.20,28.58	−80.01,−17.78	9.670	0.0085
PbG lead-glass upstream face	−43.61,35.69	−64.64,−18.42	9.730	
$B5D7$-$30D72$ entrance	−50.80,25.40	±15.24	11.608	
$B5D7$-$30D72$ exit	−50.80,25.40	±15.24	13.437	
PP counter	−53.34,27.94	±17.78	13.970	0.0161
SRX1 spark chamber	−53.34,27.94	±20.32	14.043	0.0020
SRY1 spark chamber	−53.34,27.94	±20.32	14.016	
SRX2 spark chamber	−53.34,27.94	±20.32	14.302	0.0047
SRY2 spark chamber	−53.34,27.94	±20.32	14.384	
$C\pi 2$ Cherenkov entrance	−63.50,30.48	±25.40	14.554	0.0314
$C\pi 2$ Cherenkov mirror plane	−81.28,33.02	±25.40	16.383	0.0092
$C\pi 2$ Cherenkov exit	−91.44,30.48	±25.40	16.434	0.0314
SRXY3 spark chamber	−93.98,33.02	±21.59	16.606	0.0016
SRXY4 spark chamber	−99.06,22.86	±21.59	16.856	0.0016
SRUV5 spark chamber	−109.22,33.02(u)	−62.23,34.29(v)	17.011	0.0024
HRX counter hodoscope	−88.90,12.7	±20.32	17.426	0.0847
HRY counter hodoscope	−88.90,12.7	±20.32	17.502	
HRB counter hodoscope	−88.90,12.7	±20.32	17.563	

ter elements was defined with respect to the neutral beam. Positive z is along the beam axis in the direction of the beam with $z=0$ at the target 50.8 cm upstream of the collimator entrance. Positive y is in the upward vertical direction, and positive x forms a right-handed coordinate system in the "beam left" direction. Apertures and positions of the various spectrometer elements are summarized in Table I, listing lower and upper limits in x and y, and distance from the target in z. The last column, L/L_{rad}, is the thickness in radiation lengths of each element, including one-half the thickness of air on either side of each element where appropriate. This was used for multiple Coulomb scattering in the Monte Carlo programs and to calculate the photon loss due to conversion in the spectrometer. The Cherenkov counter $C\pi 2$, which appears in Figs. 1 and 2 and in Table I, was not used in this experiment.

The spectrometer was configured in three sections, each with a bank of spark chambers to record the charged-particle tracks in that section. There were 28 planes of spark chambers, 12 x view, 12 y view, and 4 uv planes, rotated 20° with respect to the xy axes. The information from these uv chambers helped resolve ambiguities in matching x and y tracks during reconstruction. These

chambers were designated *S* (for spark chamber), followed by *F*, *M*, or *R* (for front, middle, and rear), *X*, *Y*, *XY*, or *UV* to indicate the planes contained in each chamber, and a number indicating the position in a particular bank (as in Table I). The front and rear chambers used a capacitive-readout system,[25] the middle chambers a magnetostrictive-readout system.[26]

The two spectrometer magnets *B5D6* and *B5D7* were used for momentum analysis of the pion and proton, respectively. *B5D6* was a 72*D*18 magnet, a dipole magnet with a 1.83-m-wide aperture, a pole face 45.7 cm deep, and a field integral of 0.325 T m. *B5D7* was a 30*D*72 magnet (76.2 cm wide and 1.83 m deep) with a field integral of 2.72 T m, providing momentum analysis for the higher-momentum proton.

Signals from the hodoscopes in each section were used to form a trigger indicating the presence of two tracks in the spectrometer. The spark chambers were then fired and the event was recorded. Further details of the trigger will be presented below.

A. The lead-glass array

Since the detection and identification of photons is an essential feature of this measurement, a somewhat detailed description of this portion of the apparatus is appropriate. The lead-glass array consisted of 84 pieces of lead glass arranged to form a wall. Each piece of lead glass was 6.35×6.35 cm^2 in cross section and 59.2 cm long. The blocks were oriented with the long axis parallel to the neutral beam with a photomultiplier tube connected to the downstream end of the glass.

All of the blocks were constructed from SF-2 leaded glass manufactured by Schott Optical Glass, Inc.[27] SF-2 is 50% lead oxide by weight with a density of 3.86 g/cm^3, a radiation length of 2.84 cm, and an index of refraction of 1.65. Although the blocks were made from the same material, the array was constructed with individual counters of three distinct types, each one differing slightly in assembly techniques and in the phototube employed, as described below.

A sketch of the lead-glass array is shown in Fig. 3(a) and a sketch of the different types of lead-glass blocks is shown in Fig. 3(b). The central portion of the array consisted of forty blocks (type I) in an eight-block-by-five-block arrangement. Around these on three sides were twenty blocks (type II). Finally, twenty-four blocks (type III) were arranged around the 60-block core.

Both the type-I and -II blocks had small lead-glass pipes (3.81-cm-square cross section and 10.2 cm long) glued to the downstream face of the main lead-glass blocks. These light pipes served not only as the transition to the photomultiplier tube but allowed a cylindrical magnetic shield to be located on the photomultiplier tube (extending typically 1.9 cm beyond the photocathode). This precaution was taken even though measurements of the fringe field of the two spectrometer magnets indicated a negligible contribution at the location of the array.

The type-I blocks were assembled with Kodak HE-80

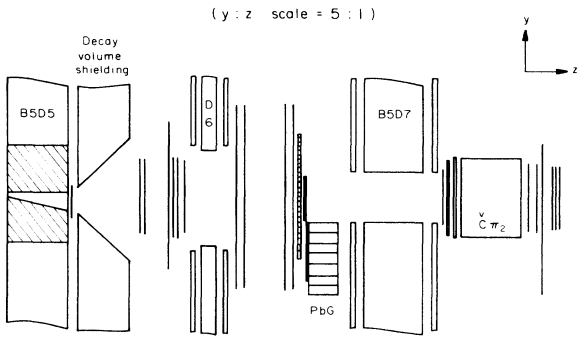

FIG. 2. Elevation view of the spectrometer. The ratio of the horizontal to vertical scale has been changed to emphasize the vertical acceptance of the apparatus. The asymmetric nature of the vertical acceptance for photons from Σ^0 decay in the lead glass (PbG) should be noted.

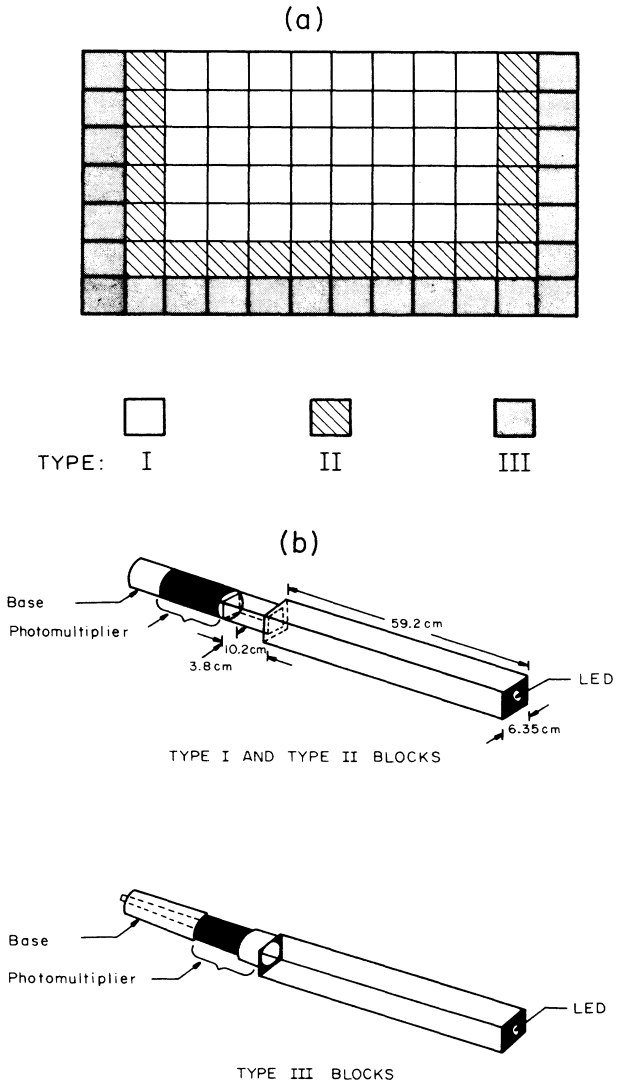

FIG. 3. The lead-glass array. (a) The arrangement of the array showing the placement of the three types of blocks. (b) A sketch of the various types of lead-glass blocks used in the array.

optical cement,[28] chosen for its index of refraction (1.544 when cured) and high transmittance in the ultraviolet wavelengths. HE-80 proved to be difficult to mix reliably in small batches, yielding problems with mechanical strength. These blocks were polished on all surfaces and had RCA 8575's (Ref. 29) glued to the downstream face of the light pipes.

The type-II blocks were assembled with Kodak HE-10 cement with an index of refraction of 1.58. All of the surfaces of the blocks were polished except the face opposite the photomultiplier tube, which was left in its ground glass state to reduce its reflectivity and thus avoid undue lengthening of the pulse. The type-II blocks utilized Amperex XP2020's (Ref. 30).

The type-III blocks, graciously loaned to the experiment by our colleagues at the University of California at Santa Barbara, used RCA 6342 (Ref. 29) photomultiplier tubes. These blocks were polished on all surfaces with a threaded collar glued to the downstream end in which a 5.1-cm diam photomultiplier tube was mounted. Optical contact was made between the tube and the glass with optical grease.

All blocks were wrapped with 0.076 mm of aluminum foil and 0.127 mm of black electrical tape to form a light seal. The high voltage for the photomultiplier tube bases was supplied with LRS HV4032 power supplies[31] which allowed individual control of each counter. All of the blocks were equipped with a 1.0-cm black bakelite plate attached to the upstream face of the glass. A calibration light source, a green gallium phosphide light-emitting diode (Monsanto MV 5222 LED) (Ref. 32), was mounted in the plate. In order to provide stable light outputs, each LED had been run for at least 40 h with a 40 mA current. In addition to the LED's, ten of the blocks had ^{241}Am-NaI sources attached on a surface of the lead-glass light pipe near the photocathode. These sources were platinum foil with a layer of diffusion-bonded ^{241}Am, an α emitter, covered by a thallium-activated NaI scintillator. Each source provided about 10 counts/sec. The LED's and the ^{241}Am sources allowed cross-checks on the stability of the gain of the photomultipliers.

The shower energy deposited in each block was measured by integrating the photomultiplier anode current pulse over a 150-nsec time window with an LRS 2249A analog-to-digital converter (ADC) (Ref. 31) on each block. The 1024-channel full scale of the ADC corresponded to a charge of 256 pC. The initial conversion factors from ADC reading (the digital value minus the ADC pedestal) to the energy of the incident particles were obtained from calibration runs in an electron test beam. Two calibration runs were conducted, one before data taking and one after.

Each block and its readout electronics was calibrated in the AGS *B*4 test beam at electron momenta of 1.5, 2.0, and 2.5 GeV/*c*. Electron identification was obtained both with a Cherenkov counter and by time of flight. The voltage on each photomultiplier tube base was adjusted so that the dynode signal from 1.5 GeV/*c* electrons had the same pulse height, allowing each block to contribute equally to a trigger pulse formed from the dynode pulses. This pulse height corresponded to an anode output which would appear near channel 400 in the ADC ($\sim$100 pC).

Before calibrating a counter, each photomultiplier was maintained on high voltage for about 24 h to allow the tube and base to reach thermal equilibrium. Measurements were taken with beam alone, with the LED pulser when the beam was off, and with the LED pulser when the beam was on. These measurements, coupled with studies of the ADC pedestals, permitted an examination of the rate dependence and linearity with energy of the lead-glass counter output.

The ratio of the LED average pulse height with beam on to the LED average with beam off represents an estimate of the gain shift with beam intensity. Gain shifts at the intensity used during the experiment were less than 1% in type-I and -II counters and on the order of 3% for type-III counters.

The calibration data also provided a measure of the energy resolution in a single block. The average energy resolution measured in the electron test beam, $\Delta E/E$, is given by the rms width of the ADC distribution divided by the average pulse height. For type-I and -II blocks, the average $\Delta E/E$ for the two calibration runs was $7.0\pm0.3\%$ and $8.0\pm0.6\%$. For type-III blocks, $\Delta E/E$ was $10.6\pm1.2\%$ and $10.8\pm1.1\%$

Since the intensity in the beam of the main experiment was relatively low, there was no expectation that the lead glass would lose transparency due to radiation effects. A comparison between calibrations done before and after the experiment confirmed that expectation. (For further discussion of the calibration procedures and comparisons with shower calculations, we refer the reader to Ref. 23.)

B. Event triggers

Several banks of scintillation counters were used to develop an electronics trigger indicating the presence of two tracks in the spectrometer. The elements that were used in the trigger included the veto counter *V*; a bank of counters upstream of *B*5*D*6, the *HFX* counters; several banks located between *B*5*D*6 and *B*5*D*7, the *HMX*, *HMB*, *HMS*, *P*, and *PP* counters; and a final set of counters located downstream of *B*5*D*7, the *HRX*, *HRY*, and *HRB* counters. This "two-track trigger" also permitted the efficiencies of the hodoscope elements to be determined from the data. The specific requirements imposed on the elements are as follows. One of the charged particles had to pass through the aperture of *B*5*D*7 and the other had to be detected in the counters between *B*5*D*6 and *B*5*D*7. Thus, the two-track triggers were

$$2\mathrm{TA}=\bar{V}\cdot P\cdot PP\cdot HFX\cdot[(HMX\cdot HMB)+HMS]\cdot(HRX\cdot HRY\cdot HRB)\ ,$$

$$2\mathrm{TB}=\bar{V}\cdot P\cdot PP\cdot HFX\cdot[(HMX+HMB)+HMS]\cdot[(HRX\cdot HRY)+(HRX\cdot HRB)+(HRY\cdot HRB)]\ ,$$

where the OR requirements in the 2TB triggers were used to extract counter efficiencies.

The triggers selected to be written onto magnetic tape consisted of three types: (1) the Λ/N trigger—the 2TB trigger prescaled by 64; (2) the Σ trigger—a coincidence between the 2TA requirement and a signal from the lead glass described below; and (3) an LED trigger generated by a computer-controlled counter test system.[33] The LED trigger permitted the continuous on-line monitoring of the performance of all hodoscope elements and trigger logic.

The lead-glass signal was formed as follows. The anode pulses from each photomultiplier were sent directly to ADC's to be digitized and recorded. The dynode signals were used to form the trigger. The voltages of the counters in each array were set during calibration so that a threshold on the sum of the dynode pulses represented an energy threshold for the showers. Only the core blocks were used in the lead-glass trigger. Signals from the inner core blocks required amplification, while signals from the outer core did not. Consequently, dynode pulses from the inner and outer core blocks were mixed separately, adjusted to give the same pulse height for a given energy, and then mixed together before a discriminator threshold was applied. A threshold of 40 mV was chosen representing an energy threshold of roughly 0.5 GeV. There was a veto counter directly in front of the array to eliminate events with charged particles entering the glass. The veto counter V_F had two phototubes which were used in OR mode. If PbG denotes a pulse from the glass above threshold, the Σ trigger requirement can be written

$$\Sigma = \mathrm{PbG}\cdot(\overline{V_{F_1}+V_{F_2}})\cdot 2\mathrm{TA}\ .$$

C. Data acquisition

When these trigger conditions were satisfied, the chambers were fired and the information was recorded on magnetic tape. Approximately 5×10^6 Σ triggers and 1.3×10^6 Λ/N triggers were recorded. (The chambers were not fired when the LED triggers occurred.)

Data acquisition was controlled by a Data General NOVA 840 computer[34] equipped with background/foreground architecture, two disk drives, two tape drives, and connected through a branch driver to two CAMAC crates. Information recorded during the beam spill was stored in memory and then written on magnetic tape in the interval between spills. An on-line reconstruction program running in the background mode processed a sample of events and monitored the operation of the equipment, signaling the operator if a malfunction was detected. Individual event reconstructions, counter and chamber efficiencies and some physics quantities were available for display. Data were taken at a rate of approximately eighteen triggers per beam spill.

The neutral beam intensity was monitored using a triplet of scintillation counters interleaved with aluminum. Care was taken to measure the accidental rates in these counters accurately.

Chamber efficiencies were constantly monitored by the on-line program using reconstructed Λ events. The overall chamber efficiency throughout the experiment was about 97%. Since both Λ^0 and Σ^0 events used the chamber information in the same way, the small event loss due to chamber inefficiency did not affect the production-ratio measurement. Voltages on the counters and the lead glass were checked periodically, usually once every eight-hour shift, as were the thresholds on the lead-glass trigger discriminators. The currents in all the beam and spectrometer magnets were monitored by the Brookhaven DIBBUK system.[35]

The data record was written after each spill. In addition to the record length and the number of events included, the data record contained the following.

Digital voltmeter (DVM) readings. The three magnets in the neutral beam line were each equipped with Hall voltage monitors, the output of which were recorded each spill.

Scalers. Thirty-six channels of CAMAC scalers (LRS 2551) (Ref. 31) were used. The scalers were enabled only during the beam spill and were reset at the beginning of each run.

Events. Each event in the record buffer contained the following.

(1) Information from 120 ADC channels.

(2) 24 time-to-digital-converter (TDC) channels. The lead-glass arrays, hodoscope banks, and the individual proton counters were connected to CAMAC TDC's (LRS2228A) (Ref. 31). The TDC's were used to digitize the time interval between the trigger pulse and pulses from scintillation counters. The dynode signals from the lead-glass array were connected to eight TDC's in such a fashion that neighboring blocks would appear on different TDC channels.

(3) 144 latches. All the scintillation counters in the experiment were connected to latches (LRS2341S) (Ref. 31) so that every counter hit in each event was recorded. This arrangement allowed hodoscope efficiencies to be measured on and off line by projecting reconstructed tracks to the hodoscope planes and checking the appropriate latch. The trigger type for each event was also recorded in a latch.

(4) Capacitive readout information, for the front and rear spark chambers. Each spark-chamber plane was read out into one of four scanners, which generated a control word containing the number of sparks in all the chambers in the scanner, followed by the last wire number and width of each spark. Up to 64 sparks in each scanner were recorded in this fashion.

(5) Magnetostrictive readout information, for the middle chambers. Up to ten sparks in each chamber plane, including one fiducial pulse, were recorded.

An additional record was written at the beginning and at the end of each run, containing the tape and run numbers, date and time of day. About 30 000 triggers filled a data tape. The polarity of the sweeping collimator magnet was reversed every two or three runs, so that the numbers of triggers in each polarity were at any given time approximately equal. Altogether 259 tapes were written, of which 220 were data tapes. As mentioned above, about 5×10^6 Σ triggers and 1.3×10^6 Λ/N triggers

were recorded.

In addition to the normal data taking runs, some data were taken periodically with special conditions. Chief among these were magnet-off data to establish the geometry of the chamber system, checks on the efficiency of the various hodoscope banks, and additional calibration information.

D. Data analysis

The analysis of the data was done in three stages. In the first stage or primary analysis, a pattern-recognition program searched for the charged-particle tracks in the chambers. Events that did not contain at least two tracks, one a short track through the first two sections of the spectrometer (corresponding to a possible pion) and one a long track through the entire spectrometer (corresponding to a possible proton), were dropped from the data sample. In the second stage or secondary analysis, the data sample was reduced by rejecting events which did not satisfy minimum requirements for $\Lambda^0 \rightarrow p\pi^-$ decay. LED triggers were analyzed to give average pedestal and LED information for each run and dropped from the data sample as well. In the third stage or tertiary analysis, further cuts identifying clear $\Lambda^0 \rightarrow p\pi^-$ decays were made, creating the final samples from which the production ratio was determined. Reconstruction of Σ^0 events was done only in this final sample. At each stage, care was taken to treat Λ/N triggers and Σ triggers alike, with particular attention to the effect of cuts on both trigger types. Since the production ratio determination is a comparison of the number of events of each type observed when possible biases have been measured or removed, such cuts directly affect the result. Similarly, procedures for reconstructing Σ^0 events have the same potential for biasing the production ratio and will be discussed separately.

The primary analysis was performed using the Brookhaven CDC 7600 computer. Details of this pattern-recognition program have been described elsewhere[23] and will not be repeated here. As indicated above, events which had at least two tracks were written on secondary tape. The fraction of triggers satisfying this two-track-reconstruction requirement was 25.8% for the Λ/N sample and 16.7% for the Σ sample averaged over the experiment. The difference between the samples was not due to an inadequacy of the reconstruction algorithms. Detailed studies show that the Σ trigger enhances the relative fraction of spurious events in the sample. Events that failed the two-track-reconstruction requirement were found, for example, often to have no tracks in the upstream portion of the spectrometer. Thus, this difference in the reconstruction rate had no effect on the production-ratio measurement.

The secondary analysis reduced the data sample by eliminating the LED triggers and by selecting events with a clean Λ^0 decay. The cuts used to make this selection are as follows.

(1) The two tracks had to be of opposite charge with the long track being positive.

(2) $1.105 < M_{p\pi} < 1.125$ GeV/c^2. The invariant mass of the two tracks assuming a $p\pi^-$ decay is shown in Fig. 4. Since the standard deviation of the distribution was less than 2 MeV/c^2 at this stage in the analysis, this cut

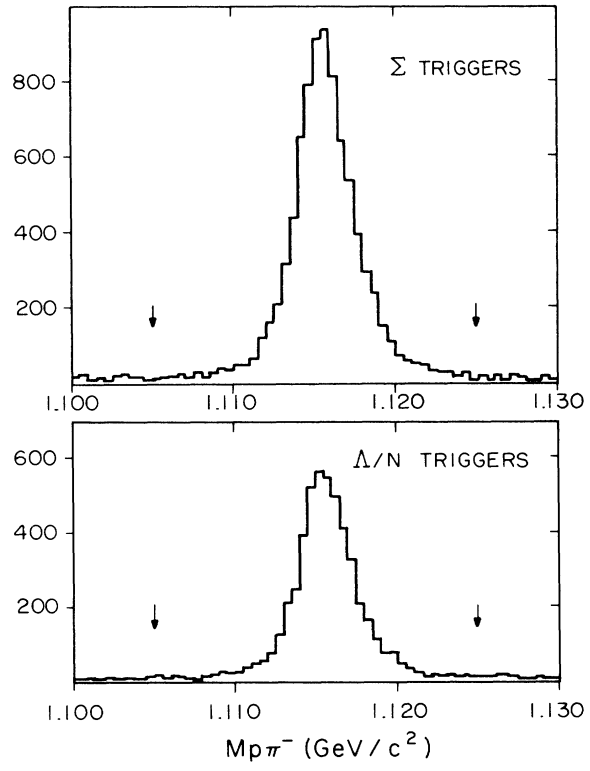

FIG. 4. Invariant-$p\pi^-$-mass distributions for each of the trigger types at the secondary analysis stage. In each a clear Λ^0 peak is evident. The arrows indicate the loose cuts imposed at this point in the analysis.

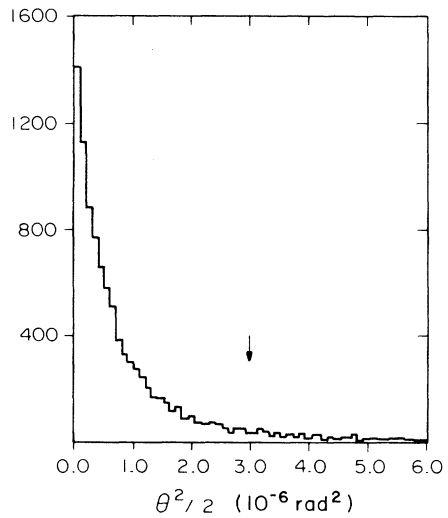

FIG. 5. $\theta^2/2$, where θ is the angle between the Λ^0 momentum vector and a line from the center of the target to the decay point. The arrow shows the position of the cut used.

($\pm 5.5\sigma$) was fairly loose.

(3) $\theta^2/2 < 3\times 10^{-6}$ rad^2. In order to require that the Λ^0 had been produced in the target, the Λ^0 momentum vector was extrapolated from the decay point at $z=z_v$ to the target. The deviation of this point from the target center, d, subtends an angle θ at the decay vertex of

$$\cos\theta \sim 1-\theta^2/2 = 1-d^2/z_v{}^2 .$$

The distribution of $\theta^2/2$ is shown in Fig. 5. The cut at 3 μsr corresponds to $d\sim 7.6$ mm, slightly larger than the target's x projection. The cut affected the Λ/N triggers more than the Σ triggers. A broad source of Λ^0's was evident at the target for Λ/N triggers, and was largely absent from the Σ triggers. This source was consistent with Λ^0 production in the beam-dump area of the collimator. A $\theta^2/2$ cut of 30 μsr eliminated the contribution from this source, and tighter target pointing cuts did not change the ratio of Σ^0's to Λ^0's significantly.

(4) $z_v = 2.74$–4.27 m. The z_v distribution (Fig. 6) shows an enhancement of track vertices at the positions of various pieces of apparatus. The cuts eliminated such effects. The windows of the decay volume were at 2.67 and 4.27 m.

(5) $S < 2.5\times 10^{-3}$ (Fig. 7). S is defined as the distance of closest approach of the two tracks normalized to the distance from this point to the middle of the front chambers, $z=5.13$ m. S is determined only by the chamber resolution and multiple scattering in the decay region and front set of chambers.

These cuts were applied to 66 000 triggers taken with the target out of the beam to determine the fraction of the secondary level data arising from other sources. About $0.26\pm 0.06\%$ of the 6500 target-out Σ triggers passed through secondary level cuts and $0.10\pm 0.01\%$ of the 59 500 Λ/N triggers, compared to a survival rate of 4.7% and 7.8%, respectively, for the target-in data. Given the relative trigger rates for target-out to target-in events (6% for Σ and 23% for Λ/N) the fraction of data arising from sources other than the target was 0.3% for both Σ and Λ/N triggers, completely negligible with respect to other backgrounds in the experiment.

LED events were also eliminated to save space. The LED events provided continuously updating averages for the ADC pedestals and the phototube gain on the LED light output. ADC pedestals, particularly the pedestals on the ADC's connected to amplifiers, were observed to shift by as much as 10 counts during the course of a run (about 40 MeV in the photon energy determination), and as much as 80 counts over the course of the experiment. A pedestal updating scheme of averaging each new pedestal value with the current average in a ratio of 1:10 followed these shifts without following the random variations of the pedestal itself. The standard deviation of the updated pedestal distribution was less than 2 counts for most of the amplified blocks. ADC pedestals for the other blocks were stable, with a width of the pedestal distribution approximately $\frac{1}{2}$ count in all cases.

The current pedestal average was subtracted from each ADC and the resulting values were written to tertiary tape. As the secondary tapes were processed, averages and standard deviations for both pedestals and LED pulse heights (the LED ADC values with the current pedestals subtracted) were recorded on a separate file. The averages from the run at the end of one secondary tape were used as input to the processing of the next run.

In the final or tertiary stage of analysis, the event selection and final corrections to the data sample were performed. Initially, the 2TA requirement was imposed in the software on both sets of triggers to reduce any possible effect of hodoscope inefficiency on the measurement of the production ratio. The entire data sample was, of course,

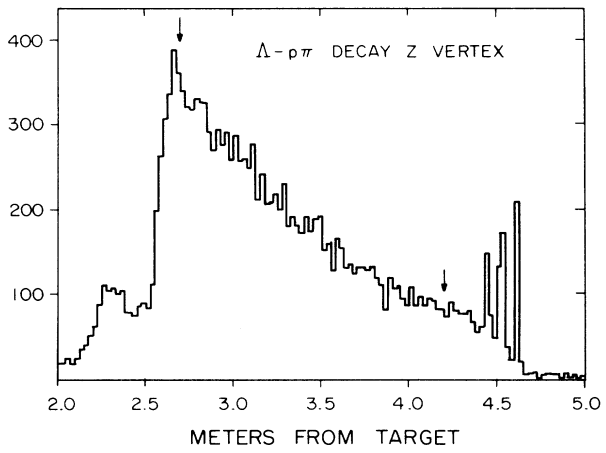

FIG. 6. The location of the decay vertex on the z axis. The peak near 2.4 m is due to the veto counter and the peaks near 4.5 m are interactions in the first chamber planes. The location of the cuts used are shown by the arrows.

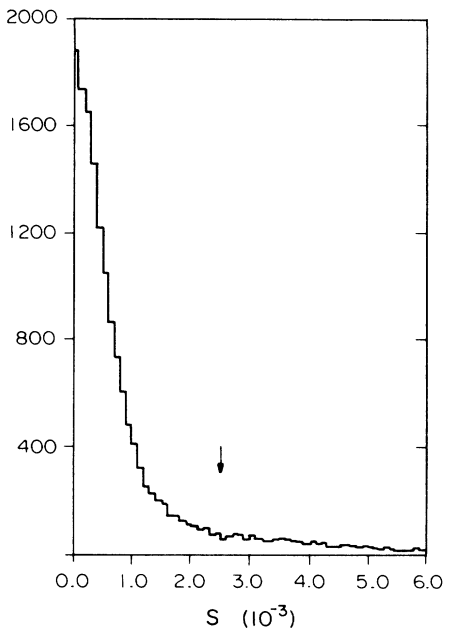

FIG. 7. S, the distance of closest approach of the two tracks normalized to the distance from the point of closest approach to the middle of the front chambers. The arrow shows the location of the cut used.

used to determine the hodoscope inefficiencies directly and those inefficiencies were used in the Monte Carlo simulation of the experiment.

The selection of the final data sample involved a tighter $M_{p\pi}$ requirement for a Λ^0 ($1.1076 < M_{p\pi} < 1.1246$ GeV/c^2) and required that all tracks pass well within the magnet and detector apertures. Before cutting on the invariant-mass distributions, the magnetic field integrals for the spectrometer magnets were updated using the Hall voltage DVM readings recorded with each event. Although the exact shape of the Λ^0 invariant-mass distribution was sensitive to this improvement in the magnetic field integrals, the number of events lost or gained from the total sample with reasonable variations in the parameters of the updating procedure was less than 0.1%. After this updating procedure was completed, the mean of the Λ^0 invariant-mass distribution was observed to shift by about 0.6 MeV/c^2 as a function of Λ^0 momentum in the 12-GeV/c Λ^0 momentum interval covered by the experiment. The uncertainty in the pion momentum indicated by this shift is approximately 0.5%, negligible with respect to the 2% Λ^0 momentum resolution.

The final $M_{p\pi}$ invariant-mass distribution for both triggers are shown in Fig. 8. For all trigger types, this distribution was found to have a mean of 1.1156 GeV/c^2 with a 1.9 MeV/c^2 standard deviation. The background under the Λ^0 mass peak, estimated by extrapolating the number of events per bin in the tails under the entire distribution, was about 1.5% of the total number of events, consistent with previous estimates of background observed in this spectrometer.[2]

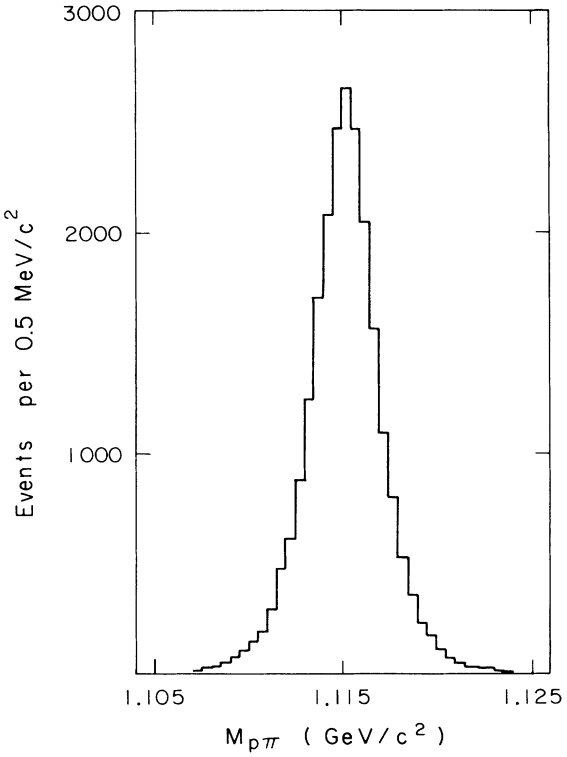

FIG. 8. Invariant-$p\pi^-$-mass distribution after applying cuts and after correcting for slow variations in the magnetic-field integrals.

The Σ^0 events in the Σ sample were extracted as follows. For each Σ trigger that contained a Λ^0 satisfying the cuts described above, the information in the lead-glass array was examined for the existence of an electromagnetic shower. Using the method to be described below, the energy $E\gamma$ and momentum vector $P\gamma$ for the photon which caused that shower was determined. The value of the $\Lambda\gamma$-invariant mass

$$M_{\Lambda\gamma}{}^2 = M_\Lambda{}^2 + 2E_\gamma(E_\Lambda - P_\Lambda \cos\theta_{\Lambda\gamma})$$

was then calculated where $\theta_{\Lambda\gamma}$ is the angle in the laboratory between the Λ^0 and the photon momenta, $\cos\theta_{\Lambda\gamma} = \hat{\mathbf{p}}_\Lambda \cdot \hat{\mathbf{p}}_\gamma$. The distribution of this invariant mass was then examined to find $\Sigma^0 \to \Lambda^0 + \gamma$ decays.

In the calculation of the $\Lambda\gamma$-invariant mass, the Λ^0-particle mass was fixed at 1.1156 GeV/c^2. The photon energy and momentum vector were determined from the lead-glass information:

$$E = \sum_{i=1}^{N} E_i = \sum_{i=1}^{N} (a_i - z_i)c_i = \sum_{i=1}^{N} p_i c_i \ ,$$

where E_i is the energy deposited in the ith block; $a_i - z_i$ is the number of ADC channels above the pedestal, or the pulse height p_i; and c_i is the calibration constant relating ADC channels to energy. The photon direction is given by the vector from the point of origin of the Λ^0 in the target to the energy centroid of the shower, the average of the participating block centers weighted by the energy deposited in each.

In determining the energy deposition in each block the pedestals used were the pedestal averages generated during secondary analysis. To avoid adding spurious energy to the shower from fluctuations in the pedestal, ADC values within twice the rms width of the pedestal distribution from the average were considered to be pedestals, and the energy in these blocks was set to zero. Negative energies were also set to zero. Events with ADC overflows in the array were removed from the sample. Further analysis of the events rejected by these cuts failed to show any evidence for Σ^0's above background.

Pedestal widths were on the order of 2 ADC counts. The minimum ADC value requirement sets a lower limit on the energy observable in any one block, just as the 1024-count full scale of the ADC supplies an upper limit. The energies to which these limits correspond depend on the particular pedestal, pedestal width, and calibration constant for each block. Using average values for these, the single-block limits on detectable energy were about 15 MeV to 3.2 GeV. The trigger threshold imposed a limit on the energy in the entire array, and hence a lower limit on the energy of the detected photon. Again, the value of the threshold energy depended on pedestals and calibration constants, but was approximately 0.5 GeV over the course of the experiment. Photon energies for Σ^0 decays detectable in this beam range from about 0.9 to 3.8 GeV. Since the energy is usually shared among several blocks, these photon energies were within the limits of the trigger

threshold and the ADC scale.

The procedure to find the showers in the lead glass was as follows. Since the minimum detectable energy in a single block was 15 MeV, studies indicated that 98% of the energy would be contained in a three-by-three array surrounding the shower. Including more blocks than these nine increased the probability of including energy unrelated to the shower to an unacceptable level. Showers were therefore reconstructed using the nine blocks only. The shower center block was taken to be the block with the maximum energy in the array. Events in which the maximum block was an edge block were eliminated. This cut removed about one-third of the events, 95% of which were in the top row of trigger blocks.

The energy contained in each block was obtained by multiplying the ADC pulse height by a calibration constant. A first approximation to these constants was provided by the test-beam data. The resulting $\Lambda\gamma$-invariant-mass distribution is shown in Fig. 9(a). Two adjustments were made to the initial constants: a change in the absolute energy scale to reproduce the Σ^0 mass at 1.1924 GeV/c^2, and an improvement of the mass resolution by following the gain shifts of individual blocks in time. Several methods were employed for these purposes during the course of the experiment. The most successful method involved calibrating on the Σ^0 mass itself. Since there is always danger in adjusting calibrations by looking at the signal, the details of the procedure used are described in some detail below as well as some of the checks of the selection process.

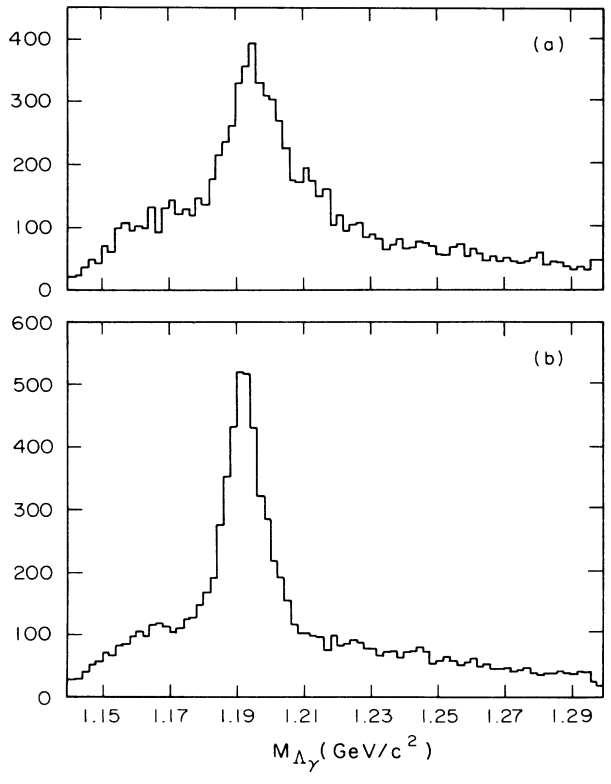

FIG. 9. Invariant-$\Lambda\gamma$-mass distribution (a) using calibrations for lead-glass blocks from test beam studies, (b) after recalibration procedure—see text. A Σ^0 signal is evident.

The procedure was a least-squares fit for the constants in a nine-block shower to produce the appropriate photon energy for a given event, that is

$$M_{\Lambda\gamma}{}^2 = M_\Lambda{}^2 + 2E_\gamma(E_\Lambda - P_\Lambda \cos\theta_{\Lambda\gamma}) \equiv (1.1924\ \text{GeV}/c^2)^2 ,$$

where E_γ has been defined before and is a sum over the nine blocks of the shower. If the pulse heights in the blocks not in the nine blocks are set equal to zero, the sum can extend over the entire array. The mass is fairly insensitive to $\cos\theta_{\Lambda\gamma}$. Since the initial calibration constants are good enough to indicate the block with the maximum energy, the energy centroid will not shift very far as the calibration constants change. The $\Lambda\gamma$ opening angle is assumed to be independent of the c_i. Thus the c_i for each event j is

$$\frac{M_\Sigma{}^2 - M_\Lambda{}^2}{2(E_{\Lambda j} - P_{\Lambda j}\cos\theta_{\Lambda\gamma j})} \equiv E_j = \sum_{i=1}^{N} p_{ij} c_i .$$

It is then desired to find the values of c_i for which deviations from this equation are minimized, i.e.,

$$\chi^2 \equiv \sum_j (E_i - p_{ij} c_i)^2$$

with each c_k such that

$$d\chi^2/dc_k = 0 = \sum_j \left[E_j - \sum_i p_{ij} c_k \right] p_{kj} = \sum_j E_j p_{kj} - \sum_i \left[\sum_j p_{ij} p_{jk} \right] c_i .$$

This is a linear system of equations where the number of equations and the number of unknowns is equal to the number of blocks in the array, and it can be solved by inverting the matrix $\sum_j p_{ij} p_{jk}$.

From Fig. 9(a) it is apparent that a large fraction of the triggers were not Σ^0 events. In order for this procedure to be meaningful, the data sample over which it is performed should contain as little background as possible. A number of cuts were investigated, in addition to the edge block cut, in an effort to reduce the background without serious loss of signal. That the background consisted primarily of photons was determined by comparing hadron showers in the data, identified by the track of the π^- from Λ^0 decay entering the glass, and electron showers from test beam studies. A cut on the ratio of the energy in the maximum energy block to that of the shower at 60% was found to eliminate 40% of the hadronic events and only 20% of the electron events. When applied to the data, with events with pions in the glass removed, this cut did not significantly improve the signal-to-background ratio in the region of the Σ^0 peak. Other cuts on shower geometry were similarly unsuccessful. A cut on the timing of the lead-glass signal with respect to the trigger was found to increase the signal-to-background ratio (before calibration, between 1.165 and 1.235 GeV/c^2) by a factor of 1.5. It should be noted that although this cut was useful in producing a clean sample for the recalibration, it was not

used in the measurement of the production ratios. Any such cut might have caused the loss of Σ^0 events.

Histograms of the $\Lambda\gamma$-invariant mass before and after calibration, appear in Fig. 9. The number of events above background was 6825 ± 560 before calibration and 7750 ± 510 after, obtained by fitting the distribution to a Gaussian for the signal plus a falling exponential for the background, over the range 1.160–1.300 GeV/c^2. The error is the sum of the statistical error on the number of events between the limits of the peak, defined to be $\pm3\sigma$, added in quadrature to the error in the integral of the background function between these limits. The width of the Gaussian signal from this fit was $\sigma=11.8\pm0.3$ MeV/c^2 before calibration and 8.7 ± 0.2 MeV/c^2 after.

Since the calibration procedure was designed to maximize the number of events in the peak, the possibility existed that the increase in the number of Σ^0 events was due to the procedure itself. Accordingly, the calibration was performed on a sample of events well away from the Σ^0 peak, in the region 1.22–1.26 GeV/c^2. The procedure tried to produce a Σ mass at 1.236 GeV/c^2; the resulting distributions, however, were merely shifted, with no suggestion of a peak being formed. The number of events near 1.236 GeV/c^2 increased by about 3% providing an upper limit on the number of spurious Σ^0's created by calibration. Further discussion of the checks performed on the procedure can be found in Ref. 23.

The photon energy resolution was determined from the Σ^0 mass resolution, assuming uncorrelated errors. The average energy resolution was 12% over the range of Σ^0 photon energies observed, compared with the 8% observed in the test beam.

A major concern in the analysis is the possibility that the procedures might preferentially lose Σ^0 events, thereby affecting the production ratio measurement. Each of the operations performed on the Σ sample was investigated to determine the size of the possible effects. Events which had been removed due to ADC overflows were reexamined, forming showers around the block with the second highest energy in the array. No Σ^0 peak was visible in the invariant-mass distributions.

Events with more than one shower were also reexamined, as there was no guarantee that the block with the maximum energy was associated with the Σ^0 photon in all cases. This second shower was required to occur outside the area of the first shower. No statistically significant enhancement of events in the region of the Σ^0 mass was observed.

The possibility was considered that the accidental overlap between a photon from Σ^0 decay and energy deposited in the array from other sources could cause the loss of a Σ^0 event. These other sources include fluctuations in various blocks as well as showers from processes other than Σ^0 decay. Because the number of Σ^0 events is determined by subtracting background, the likelihood of a reduction in signal due to the presence of extra energy is difficult to estimate. However, if a two-standard-deviation shift in $m_{\Lambda\gamma}$ is required to eliminate a Σ^0 event from the peak, the probability is about 0.5% that a Σ^0 will be lost. The nine-block shower energy could also be affected by a nearby second shower, one occurring in the sixteen-block outer ring. In order to deposit sufficient energy for a two-standard-deviation shift in $m_{\Lambda\gamma}$, this shower must have a total energy approximately equal to that of the main shower, which occurs for $\sim2\%$ of the events in the mass peak.

If the pedestals of individual blocks had not been tracked properly, the calibrations of those blocks could have been incorrect, resulting in the loss of Σ^0 events. It was estimated that such effects would not contribute more than 2%.

When all of the possible loss mechanisms were considered, and their effects added in quadrature, there is an overall estimated loss of Σ^0 events due to photon reconstruction of $3\pm3\%$.

At this point, it is appropriate to address the difference in effective live time for each trigger. The major difference was due to the lead-glass veto counter, which affected Σ triggers only. The live time for Σ triggers was approximately 1% less than that for Λ/N triggers, a small but direct contribution to the loss of Σ^0 events relative to Λ^0 events.

In order to determine the relative acceptance of the spectrometer for Λ^0's and Σ^0's, a detailed Monte Carlo simulation of the experiment was performed. For the most part, there was nothing unique about this Monte Carlo calculation and the interested reader is referred to Ref. 23 for further details. Suffice it to say that all known effects were included such as multiple Coulomb scattering, chamber resolutions and inefficiencies, counter inefficiencies, lead-glass resolution, and $\pi\to\mu\nu$ decays in flight.

In the Monte Carlo calculation, the Λ^0's were produced with the polarization measured in a previous experiment in this spectrometer, specifically

$$\mathbf{P}_\Lambda=\begin{cases}-(0.44\pm0.02)(p-0.57\pm0.04)\hat{\mathbf{n}}, & p>0.57\ \text{GeV}/c,\\ 0, & p<0.57\ \text{GeV}/c,\end{cases}$$

where p is the Λ^0 momentum transverse to the beam direction in the laboratory and $\hat{\mathbf{n}}=\hat{\mathbf{p}}_{\text{beam}}\times\hat{\mathbf{p}}_{\Lambda\,\text{lab}}$ is the normal to the production plane. For Λ^0's with polarization $\mathbf{P}_\Lambda$, the distribution of the proton in the rest frame of the Λ^0 is proportional to $(1+\alpha_\Lambda\hat{\mathbf{p}}_p\cdot\mathbf{P}_\Lambda)$ where $\alpha_\Lambda=0.647\pm0.013$ (Ref. 36) and $\hat{\mathbf{p}}_p$ is the direction of the proton.

For the purposes of the Monte Carlo simulation, the Σ^0 polarization was taken to be of the same magnitude as the Λ^0 polarization but in the opposite direction, as suggested by $\Sigma^\pm$ polarization data.[17,18] The Λ^0 resulting from the decay of a Σ^0 with polarization $\mathbf{P}_\Sigma$ will have a polarization

$$\mathbf{P}_{\Lambda_\Sigma}=-(\mathbf{P}_\Sigma\cdot\hat{\mathbf{P}}_\Lambda)\hat{\mathbf{p}}_\Lambda$$

in the Σ^0 center-of-mass frame.[37]

Finally, the Monte Carlo calculation simulated the precession of the Λ^0 in the magnetic field of the sweeping collimator.

An important factor in the Σ^0 acceptance which was not calculated directly in the Monte Carlo program was the probability of photon conversion in the target and spectrometer. Table I includes the values of L/L_{rad} for elements of the spectrometer, determined from the radia-

tion lengths of the materials used. The effective $L/L_{\rm rad}$ for the spectrometer was 0.057. In addition, the thickness of the target traversed by the photons was added. This thickness differed somewhat for each photon according to its point of origin and direction, with an average $L/L_{\rm rad}$ of 0.051 ± 0.010. This correction represented a factor of 0.87 ± 0.01 in the acceptance calculation.

The acceptances for Σ^0 and Λ^0's are not very sensitive to the polarization of the particle. For Σ^0 decay only a fraction of the polarization is transmitted to the Λ^0. Since this polarization is dependent on the angle the Λ^0 makes with the production plane normal in the Σ^0 center of mass, any effect the Σ^0 polarization may have on the $\Lambda^0\to p\pi^-$ acceptance is effectively diluted. Although there is no such dilution with Λ^0 polarization, which occurs along the production plane normal and precesses through a fixed angle in the sweeping collimator, the effect of polarization is minimal. Polarization reduces the Λ^0 acceptance only in the highest p and p_T bins. In the worst case, the acceptance only changes by 15% of its value.

III. RESULTS

The data were examined both as a function of p, the magnitude of the momentum of the produced particle, and as a function of p_T, the momentum of the produced particle transverse to the incident proton beam. In each case, the data were binned in the appropriate variable (p or p_T).

The production ratio R_1 of the cross section for Σ^0 inclusive production to the cross section for Λ^0 inclusive production was calculated in each bin as

$$R_1=\frac{N_\Sigma}{N_\Lambda}\frac{A_\Lambda}{A_\Sigma}\frac{B}{64}\ ,$$

where N_Σ and N_Λ are the number of Σ^0 and Λ^0 observed in each bin, A_Λ/A_Σ is the ratio of the acceptance of the apparatus for Λ^0 and Σ^0 decays into $p\pi^-$, and the factor 64 is the prescale factor. Since only the $p\pi^-$ decay of the Λ^0 is observed, B is the ratio of the $p\pi^-$ fraction of all Λ^0 decays to the $p\pi^-\gamma$ fraction of all Σ^0 decays. Specifically

$$B=\frac{\Gamma(\Lambda^0\to p\pi^-)}{\Gamma(\Lambda^0\to \text{all})}\frac{\Gamma(\Sigma^0\to \text{all})}{\Gamma(\Sigma^0\to\Lambda^0\gamma)}\frac{\Gamma(\Lambda^0\to \text{all})}{\Gamma(\Lambda^0\to p\pi^-)}\ .$$

Since the branching ratio for $\Sigma^0\to\Lambda\gamma$ is $\sim 100\%$, B is 1.

In each bin, the number of Λ^0 events N_Λ was determined from the Λ/N sample by the number of events passing all of the cuts minus the estimated background under the peak, typically 1.5%. The number of Σ^0 events in each bin, N_Σ, was found by fitting each $m_{\Lambda\gamma}$ histogram with a Gaussian signal plus an exponential background. The χ^2 for these fits was typically 80 for 70 degrees of freedom. The fitted background was subtracted from the data to give N_Σ. Several systematic corrections were applied to N_Σ. The corrections, described in detail above, included an estimate of the number of photons lost due to early conversion in the target or spectrometer $(13\pm1)\%$; lifetime corrections for the Σ trigger ($<1\%$); and effects due to photon reconstruction and the energy calibration procedure ($<3\%$).

The number of Σ^0 events determined by this procedure depends slightly on the choice of the background function. The coincidence of a photon in the lead glass and a Λ^0 in the spectrometer could be due to many things. For example, if the production of a Λ^0 is accompanied by the production of a π^0, one of the photons from the π^0 might be detected in the apparatus. In addition, interactions of the neutral beam in the apparatus could produce photons as well. In the analysis, a single exponential has been used as the background function for simplicity, but other hypotheses may be equally valid. Since the quality of the fits with the single exponential was quite satisfactory, very little effort was spent examining other shapes. We found that a better χ^2 could be achieved only at the expense of the addition of extra parameters and without significant changes in the result.

As discussed above, the relative acceptance for Λ^0 and Σ^0 events, A_Λ/A_Σ was calculated using a Monte Carlo program. Acceptances were determined by passing Monte Carlo generated events through the same analysis procedures used for the data and by taking the ratio of observed to generated events in each p or p_T bin. The acceptance ratio A_Λ/A_Σ decreased with increasing momentum with an average value on the order of 50.

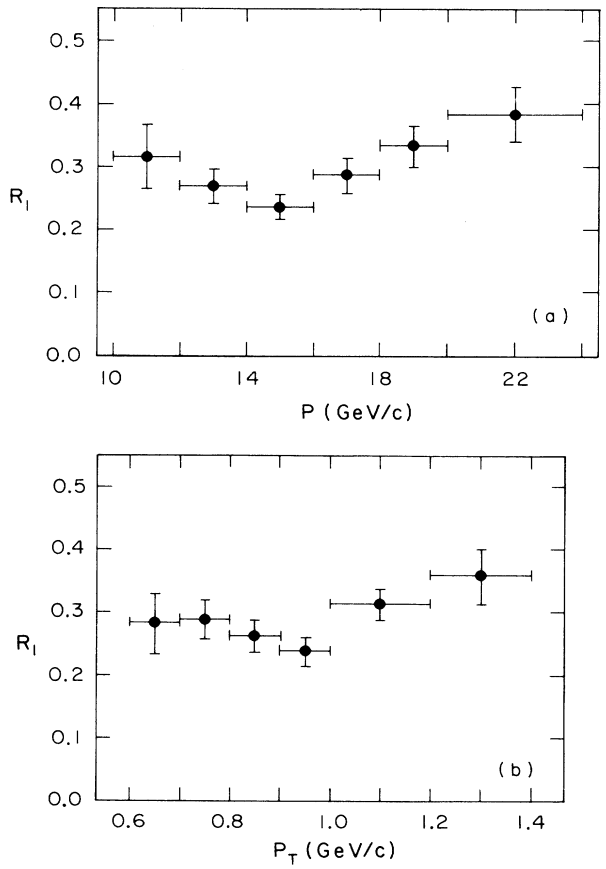

FIG. 10. R_1, the ratio of Σ^0 inclusive production to Λ^0 inclusive production, is shown vs (a) p, the momentum of the produced particle and (b) p_T, the transverse momentum of the produced particle. The errors are statistical only.

TABLE II. R_1, the ratio of inclusive Σ^0 production to inclusive Λ^0 production, given as a function of p, the momentum of the produced particles, and p_T, the transverse momentum of the produced particles. The errors shown are statistical only.

p (GeV/c)	R_1 (%)
10.0–12.0	31.57±5.14
12.0–14.0	26.87±2.79
14.0–16.0	23.56±1.88
16.0–18.0	28.70±2.40
18.0–20.0	33.11±3.22
20.0–24.0	38.44±4.40
p_T (GeV)/c)	R_1 (%)
0.60–0.70	28.23±4.56
0.70–0.80	28.81±2.95
0.80–0.90	26.23±2.33
0.90–1.00	23.77±2.09
1.00–1.20	31.35±2.30
1.20–1.40	35.82±4.31

In Fig. 10, R_1 is shown plotted against p and p_T and the values of R_1 are given in Table II. R_1 does not depend strongly on either p or p_T over the range observed. The weighted average for R_1 is $0.278\pm0.011\pm0.05$, where the first uncertainty is statistical and the second is an estimate of systematic uncertainties.

Various additional checks on this result were performed. For example, the effect of the polarity of the sweeping collimator on the result was investigated. Since the Λ^0's precess in the field of the sweeping collimator, the angular distributions of the decay products in the spectrometer depend on the polarity of the collimator magnetic field. Further, since the collimator was asymmetric in the vertical direction, the veto counter dead time was approximately 10% longer for one polarity than for the other. The value of R_1 was unaffected, however. The ratio of R_1 calculated using data from each polarity separately was 1.01 ± 0.01. Another check involved calculating R_1 by dividing the data into two sets depending on whether the photon was detected to the left or right of the beam center line in the lead-glass array. The ratio of those values of R_1 was 1.15 ± 0.15.

There was concern that the combination of the lead-glass array and the lead-glass veto counter might reject a large fraction of photons. If a photon produced a backward-going particle as it entered the lead glass, such a particle might enter the lead-glass veto counter, thereby eliminating the event. Unfortunately no substantial amount of data was taken with the veto counter removed to check on this effect. However, a detailed examination of the angular distributions and particle numbers for showers in this energy range indicate that the number of such losses is significantly less than one percent of all photons entering the array.

It should be noted that the value of R_1 includes all sources for Λ^0 production. The major contributions are "directly produced" Λ^0's, including resonance production, Λ^0's from Σ^0 decay, and Λ^0's from the decay of other strange particles such as the Ξ^0, the Ξ^-, and the Ω^-.

The size of the contribution from $\Xi^0\to\Lambda^0\pi^0$ was investigated in some detail. Using the Monte Carlo program, Ξ^0 production and subsequent decay was generated and the resulting Λ^0's were subjected to the full analysis program. Since the Ξ^0 will travel a measurable distance before decaying, a fraction of the Λ^0's from Ξ^0 decay are eliminated by the target-point back requirement, $\theta^2/2<3$ μsr. Including all cuts, the acceptance of the spectrometer for directly produced Λ^0's is roughly seven times the acceptance for Λ^0's from Ξ^0 decay. In an experiment[38] using 24-GeV/c protons on platinum at a production angle of 75 ± 13 mrad, the Ξ^0/Λ^0 production ratio was measured to be 1.2×10^{-2}, 2 m from the target. This yields an effective production ratio at the target of 0.9×10^{-2}. If we assume that this production ratio holds for this experiment, the expected contribution from this decay is 0.1%. Similar calculations indicate that the contribution from Ξ^- or Ω^- decays is also very small.

Although the decay $\Xi^0\to\Lambda^0\pi^0$ produces two photons, it is even more unlikely that this process can contribute to the Σ^0 signal. The acceptance of the apparatus for both the Λ^0 and either of the photons is significantly smaller than for just the Λ^0 alone.

In the calculation that follows, the assumption is made that there are only two significant contributions to the Λ^0 production observed in this experiment: namely, directly produced Λ^0's and Σ^0 decay Λ^0's. With this assumption,

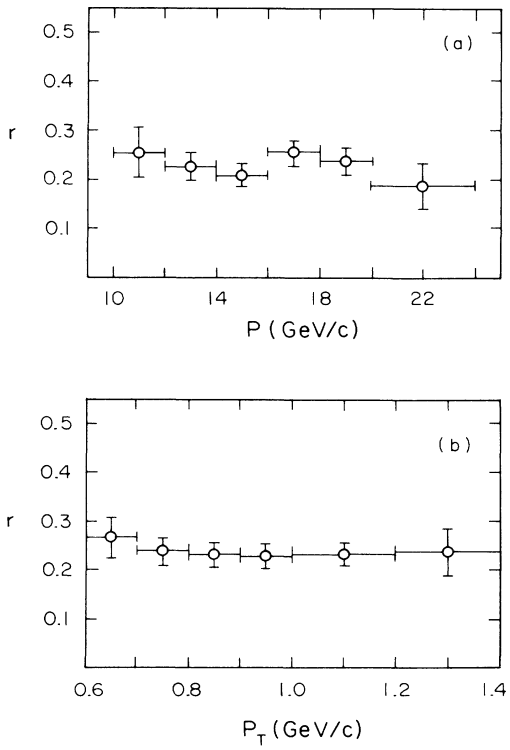

FIG. 11. The ratio r of Σ^0 decay Λ^0's to inclusive Λ^0 production, given as a function of (a) p, the momentum of the produced particle and (b) p_T, the transverse momentum of the produced particle. The errors shown are statistical only.

TABLE III. The ratio r of Σ^0 decay Λ^0's to inclusive Λ^0 production given as a function of p, the momentum of the produced particle, and p_T, the transverse momentum of the produced particle. The errors shown are statistical only.

P (GeV/c)	r (%)
10.0–12.0	25.3±4.9
12.0–14.0	22.7±2.6
14.0–16.0	20.9±2.3
16.0–18.0	25.4±2.5
18.0–20.0	23.9±2.8
20.0–24.0	19.0±4.5
p_T (GeV/c)	r (%)
0.60–0.70	26.7±4.2
0.70–0.80	23.7±2.9
0.80–0.90	23.0±2.6
0.90–1.00	22.7±2.5
1.00–1.20	23.0±2.3
1.20–1.40	23.8±4.7

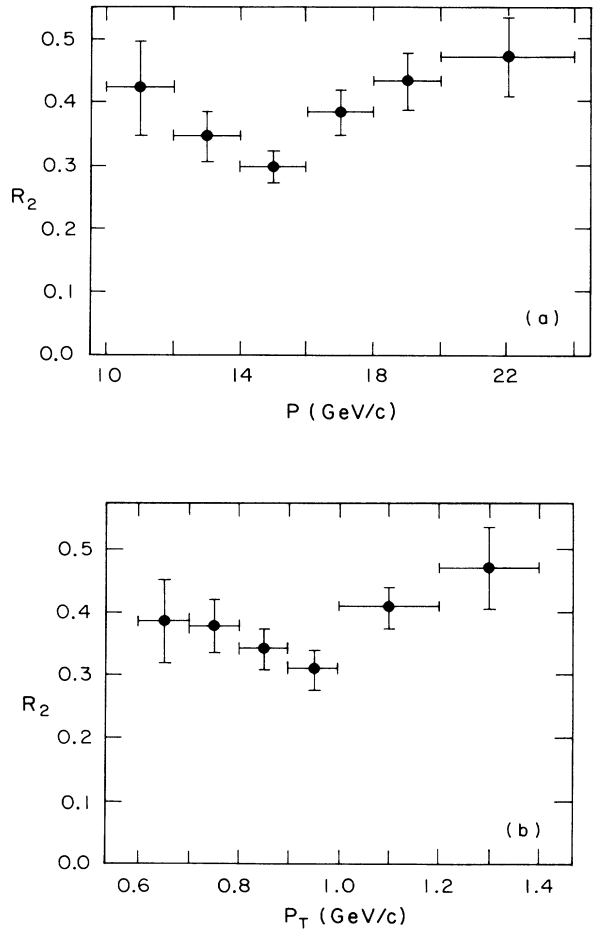

FIG. 12. R_2, the ratio of Σ^0 inclusive production to directly produced Λ^0 production, is shown vs (a) p, the momentum of the produced particle and (b) p_T, the transverse momentum of the produced particle. The errors are statistical only.

it is possible to extract a value for R_2, the ratio of the cross section for Σ^0 inclusive production to the cross section for inclusive directly produced Λ^0 production.

As a first step in that calculation, the Λ/N data were reanalyzed to determine r, the ratio of Σ^0 decay Λ^0's to the total Λ^0 production. Events with a Λ^0 surviving all cuts were examined for showers in the lead glass. The invariant-mass distributions were created as described for the Σ triggers and the number of Σ^0 events was extracted. The ratio r is obtained by multiplying the ratio of the number of Λ/N events containing a Σ^0 to the total number of Λ^0 by the relative acceptances calculated by a Monte Carlo program. In Fig. 11 the results of that analysis are shown versus p and p_T and the values of r are given in Table III.

R_2 is then calculated as

$$R_2 = R_1/(1-r) .$$

In Fig. 12, R_2 is shown plotted versus p and p_T and the values of R_2 are given in Table IV. In the range under investigation, Σ^0 production is approximately 36% of directly produced Λ^0 production.

IV. COMPARISON WITH MODELS AND CONCLUSION

These results suggest that a reanalysis of all previous measurements of Λ^0 polarization in inclusive processes is necessary. First, Σ^0 production is a large fraction of Λ^0 production. Second and more importantly, Λ^0's from Σ^0 decay retain on the average $-\frac{1}{3}$ of the Σ^0 polarization.[37] Thus, the polarization of directly produced Λ^0's can be quite different from the polarization measured for inclusively produced Λ^0's.

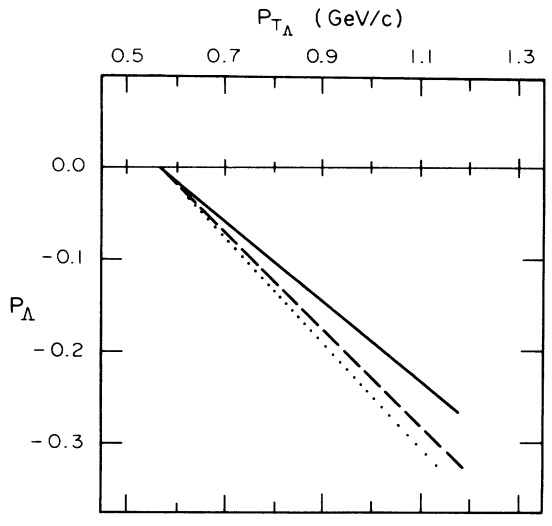

FIG. 13. The effect of this measurement on a previous Λ^0 polarization experiment. The solid line is the fit to the polarization data determined in Ref. 3. The dashed line results if Σ^0 polarization is equal and opposite to that of the observed Λ^0 polarization. The dotted line results if the Σ^0 are produced unpolarized.

TABLE IV. R_2, the ratio of inclusive Σ^0 production to directly produced Λ^0 production, given as a function of p, the momentum of the produced particle, and p_T, the transverse momentum of the produced particle. The errors shown are statistical only.

p (GeV/c)	R_2 (%)
10.0–12.0	42.2±7.4
12.0–14.0	34.7±3.8
14.0–16.0	29.8±2.5
16.0–18.0	38.5±3.5
18.0–20.0	43.5±4.5
20.0–24.0	47.4±6.1
p_T (GeV/c)	R_2 (%)
0.60–0.70	38.5±6.6
0.70–0.80	37.8±4.1
0.80–0.90	34.1±3.2
0.90–1.00	30.8±2.9
1.00–1.20	40.7±3.2
1.20–1.40	47.0±6.4

As an example of this effect, we reexamine the Λ^0 polarization measured in Ref. 3. In Ref. 3 the Λ^0 polarization is presented as a function of P_T, the transverse momentum of the Λ^0. To determine the contamination from Σ^0's as a function of P_T, our data were reanalyzed binning in that variable. The Λ^0 polarization measured in Ref. 3 was then corrected under two different assumptions regarding Σ^0 polarization. In Fig. 13 the solid line is the fit to the Λ^0 polarization data obtained in Ref. 3. The dashed line results if Σ^0 polarization is equal and opposite to that of the observed Λ^0 polarization. The dotted line results if the Σ^0's are produced unpolarized. In each case, the effect is significant.

We note that this result is the first measurement using protons of the Σ^0/Λ^0 inclusive production ratio in this energy range. It is interesting that the value of the Σ^0/Λ^0 ratio (0.278) measured with protons at 28.5 GeV/c is consistent with the value determined with incident kaons at a much lower energy[6] (0.30 at 8.25 GeV/c) and with exclusive measurements in pp interactions[20] at 6 GeV/c (0.33).

It is most striking that there is apparent agreement between all measurements of this ratio and apparent insensitivity to beam energy and beam particle type. Clearly there is not sufficient data to warrant ascribing this agreement to any fundamental mechanism, but the trend is fascinating.

On the other hand, there is a disparity between the experimental results and the theoretical predictions of this ratio. This may indicate how poorly the basic mechanisms are understood. It is perhaps amusing that the production ratio is consistent with the simple argument that Σ and Λ production are equal. Since there are three Σ's, Σ^0/Λ^0 should be roughly one-third. It is hoped that these experimental results will encourage further theoretical input.

While this experiment has addressed the contribution of Σ^0 decay, it is important to note that there are other sources of Λ^0's which are not directly produced. Chief among these sources is baryon resonance production such as the $\Sigma(1385)$. It is essential that any treatment of hyperon polarization phenomenon account for these nondirect contributions. Since the nondirect contributions are very large, one should be wary of models that naively ignore those contributions. It is entirely possible that any agreement between theory and experiment without such effects has been fortuitous.

ACKNOWLEDGMENTS

We would like to thank the Director and staff of the Brookhaven National Laboratory for their invaluable assistance. The University of Massachusetts Computer Center is also to be thanked. We are extremely indebted to our colleagues at the University of California at Santa Barbara for the loan of some lead-glass blocks. We would also like to thank Dr. T. Kycia at Brookhaven, Professor T. O'Halloran at the University of Illinois, and Professor F. Shoemaker at Princeton University for the loan of some experimental apparatus. The work was supported in part by the U.S. National Science Foundation and the U.S. Department of Energy.

*Present address: AT&T Bell Laboratories, Holmdel, NJ 07733.
†Present address: Department of Physics, Rice University, Houston, Texas 77001.

[1]G. Bunce, R. Handler, R. March, P. Martin, L. Pondrom, M. Sheaff, K. Heller, O. E. Overseth, P. Skubic, T. Devlin, B. Edelman, R. Edwards, J. Norem, L. Schachinger, and P. Yamin, Phys. Rev. Lett. **36**, 1113 (1976).

[2]F. Lomanno, D. Jensen, M. N. Kreisler, R. Poster, M. S. Z. Rabin, M. Way, J. Wise, and J. Humphrey, Phys. Rev. Lett. **43**, 1905 (1979).

[3]K. Raychaudhuri, D. Jensen, F. Lomanno, D. McIntyre, M. Rabin, G. Bunce, S. P. Yamin, P. T. Cox, J. Dworkin, O. E. Overseth, K. Heller, and Y. Makdisi, Phys. Lett. **90B**, 319 (1980).

[4]S. Erhan, W. Lockman, M. Medinnis, T. Meyer, J. Rander, P. Schlein, R. Webb, A. Boehm, H. Foeth, A. Staude, R. Ellis, B. Naroska, P. Strolin, and J. Zsembery, Phys. Lett. **82B**, 301 (1979).

[5]M. L. Faccini-Turluer, R. Barloutaud, C. Cochet, A. Givernaud, L. Mosca, J. Saudraix, P. Sixel, L. Becker, U. Gensch, E. deWolt, F. A. Triantis, R. Windmolders, H. Blumenfeld, Yu. I. Arestov, P. V. Chiapnikov, A. S. Minaeuko, A. M. Rybin, U. S. Uvarov, and J. MacNaughton, Z. Phys. C **1**, 19 (1979).

[6]M. Baubillier, I. J. Bloodworth, G. J. Bossen, A. Burns, J. N. Carney, M. J. Corden, C. A. Cowan, G. F. Cox, C. J. DeLima, D. Dixon, J. B. Kinson, K. Knudson, F. Levy, H. McCann, M. MacDermott, P. J. Negus, B. Oh, M. Pratap, E. Quercigh, M. Rivoal, J. M. Scarr, J. C. Shiers, G. Smith, D. Teodoro, O. Villalobos Baillie, M. F. Votruba, J. Whitmore, and R. Zitoun, Nucl. Phys. **B148**, 18 (1979).

[7]K. Heller, O. E. Overseth, G. Bunce, F. Dydak, and H. Taureg,

Phys. Lett. **68B**, 480 (1977).

[8]K. Heller, P. T. Cox, J. Dworkin, O. E. Overseth, P. Skubic, L. Schachinger, T. Devlin, B. Edelman, R. T. Edwards, G. Bunce, R. Handler, R. March, P. Martin, L. Pondrom, and M. Scheaff, Phys. Rev. Lett. **41**, 607 (1978); **45**, 1043(E) (1980).

[9]F. Abe, K. Hara, N. Kim, K. Kondo, S. Miyashita, H. Miyata, I. Nakano, T. Sugaya, K. Takikawa, R. Tanaka, Y. Yamamoto, T. Yasuda, K. Yasuoka, Y. Asano, Y. Iguchi, S. Mori, Y. Fukui, S. Kurokawa, and A. Maki, Phys. Rev. Lett. **50**, 1102 (1983); J. Phys. Soc. Jpn. **52**, 4107 (1983).

[10]Unfortunately, space does not permit the citing of all the excellent work in this field. We therefore refer the interested reader to both review articles and conference proceedings such as *High Energy Physics with Polarized Beams and Polarized Targets,* proceedings of the 1980 International Symposium, Lausanne, Switzerland, 1980, edited by C. Joseph and J. Soffer (Experientia Supplementum, Vol. 38) (Birkhauser, Basel, Switzerland, 1981); J. Lach and L. Pondrom, Annu. Rev. Nucl. Particle Sci. **29**, 203 (1979); L. Pondrom, Phys. Rep. **122**, 57 (1985).

[11]A. V. Efremov, Yad. Fiz. **28**, 166 (1978) [Sov. J. Nucl. Phys. **28**, 83 (1978)].

[12]B. Andersson, G. Gustafson, and G. Ingelman, Phys. Lett. **85B**, 417 (1979).

[13]G. L. Kane, J. Pumplin, and W. Repko, Phys. Rev. Lett. **41**, 1689 (1978).

[14]T. A. DeGrand and H. I. Miettinen, Phys. Rev. D **24**, 2419 (1981).

[15]M. W. Sullivan, D. A. Jensen, M. N. Kreisler, M. Marcin, K. K. Raychaudhuri, G. M. Bunce, Y. Makdisi, P. Yamin, K. Heller, E. C. Dukes, and O. E. Overseth, Phys. Lett. **142B**, 451 (1984).

[16]F. Lomanno, D. Jensen, M. N. Kreisler, R. Poster, M. S. Z. Rabin, M. Way, J. Wise, and J. Humphrey, Phys. Lett. **96B**, 223 (1980).

[17]C. Wilkinson, R. Handler, B. Lundberg, L. Pondrom, M. Sheaff, P. T. Cox, C. Dukes, J. Dworkin, O. E. Overseth, A. Beretvas, L. Deck, T. Devlin, K. B. Luk, R. Rameika, R. Whitman, and K. Heller, Phys. Rev. Lett. **46**, 803 (1981); L. Deck, A. Beretvas, T. Devlin, K. B. Luk, R. Rameika, R. Whitman, R. Handler, B. Lundberg, L. Pondrom, M. Sheaff, C. Wilkinson, P. T. Cox, C. Dukes, J. Dworkin, O. E. Overseth, and K. Heller, Phys. Rev. D **28**, 1 (1983).

[18]C. Ankenbrandt, J. P. Berge, A. E. Brenner, J. Butler, K. Doroba, J. E. Elias, J. Lach, P. Laurikainen, J. MacLachlan, J. Marriner, E. McCliment, E. W. Anderson, A. Breakstone, T. Cardello, P. S. Cooper, L. J. Teig, J. L. Thron, and Y. W. Wah, Phys. Rev. Lett. **51**, 863 (1983); G. Zapalac, S. Y. Hsueh, D. Muller, J. Tang, R. Winston, E. C. Swallow, J. P. Berge, A. E. Brenner, P. Grafstrom, E. Jastrzembski, J. Lach, J. Marriner, R. Raja, V. J. Smith, E. McCliment, C. Newsom, E. W. Anderson, A. S. Denisov, V. T. Grachev, V. A. Shegelsky, D. M. Seliverstov, N. N. Smirnov, N. K. Terentyev, I. I. Tkatch, A. A. Vorobyov, P. S. Cooper, P. Razis, and L. J. Tieg, *ibid.* **57**, 1526 (1986).

[19]See, for example, the measurement of the magnetic moment of the Σ^- hyperon in Ref. 18.

[20]W. Chinowsky, R. R. Kinsey, S. L. Klein, M. Mandelkern, J. Schultz, F. Martin, M. L. Perl, and T. H. Tan, Phys. Rev. **165**, 1466 (1968).

[21]H. Kichimi, M. Fukawa, S. Kabe, F. Ochiai, R. Sugahara, A. Suzuki, Y. Yoshimura, K. Takahashi, T. Okusawa, K. Tanahashi, M. Teranaka, O. Kusumoto, T. Konishi, H. Okabe, and J. Yokota, Phys. Lett. **72B**, 411 (1978).

[22]J. Wise, D. A. Jensen, M. N. Kreisler, F. Lomanno, R. Poster, M. S. Z. Rabin, K. Raychaudhuri, M. Way, and J. Humphrey, Phys. Lett. **91B**, 165 (1980).

[23]M. W. Sullivan, Ph.D. thesis, Department of Physics and Astronomy, University of Massachusetts, Amherst, Massachusetts, 1982.

[24]We note that due to a revision in the Monte Carlo calculations, the production cross-section ratios presented in Ref. 23 differ from our final results in Ref. 15 and the current paper.

[25]T. A. Nunamaker, Rev. Sci. Instrum. **42**, 1701 (1971).

[26]Scientific Accessory Corporation, Bridgeport, Connecticut.

[27]Schott Optical Glass, Inc., York Avenue, Duryea, Pennsylvania.

[28]Eastman Kodak Company, Rochester, New York.

[29]Radio Corporation of America, Electronics Components and Devices, Harrison, New Jersey.

[30]Amperex Electronics Corporation, 230 Duffy Avenue, Hicksville, New York.

[31]LeCroy Research Systems Corporation, 700 South Main Street, Spring Valley, New York.

[32]Monsanto Electronics Division, 3400 Hillview Avenue, Palo Alto, California.

[33]D. Jensen, M. Kreisler, F. Lomanno, R. Poster, M. Rabin, P. Smart, J. Wise, and J. Dakin, Nucl. Instrum. Methods **169**, 503 (1980).

[34]Data General Corporation, Southboro, Massachusetts.

[35]D. Lowenstein, EP&S Technical Note No. 75, Brookhaven National Laboratory, 1975 (unpublished).

[36]Particle Data Group, Phys. Lett. **170B**, 1 (1986).

[37]R. Gatto, Phys. Rev. **109**, 610 (1958).

[38]C. Geweniger, S. Gjesdal, G. Presser, P. Steffen, J. Steinberger, F. Vanucci, H. Wahl, F. Eisele, K. Kleinknecht, V. Luth, and G. Zech, Phys. Lett. **57B**, 193 (1975).

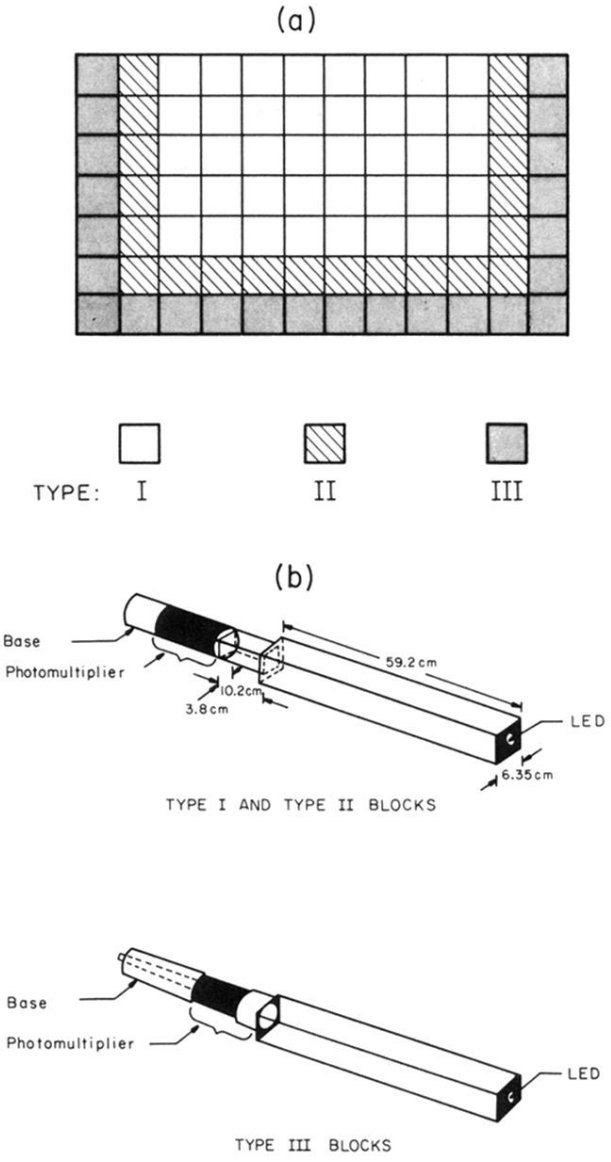

FIG. 3. The lead-glass array. (a) The arrangement of the array showing the placement of the three types of blocks. (b) A sketch of the various types of lead-glass blocks used in the array.